CANCER

Stress-induced CXCL13 regulates pancreatic exocrine homeostasis, age-related chronic inflammation, and cancer progression

Masahiro Yoshida[1,2], Kenichiro Furuyama[1,2], Keisuke Sumide[3], Masashi Horiguchi[1,2], Ahmed I. Abo-Ahmed[2,4], Hirofumi Shibata[2], Akito Tanaka[2], Ahmed M. Rashwan[2,5], Toshihiko Masui[1,2], Cantas Alev[6], Takuya Yamamoto[2,6,7], Yasuhiro Yamada[8], Shin Kaneko[3], Shuh Narumiya[9,10], David Tuveson[11], Shinji Uemoto[12], Etsuro Hatano[1], Yoshiya Kawaguchi[2]*

Pancreatic cancers, whose incidence increases with age, are often refractory to treatment. Here, we identified a core mechanism shared by physiological homeostasis, senescent cell accumulation during aging, and pancreatic cancers. Pancreatic acinar cells, when stressed, secrete CXCL13, which protects stressed cells while transiently activating paracrine Hippo/YAP signaling to induce proliferation and PD-L1–mediated immune protection to maintain organ homeostasis. In the aged pancreas, CXCL13/YAP/PD-L1 signaling permits senescent cells to survive, driving feedforward chronic inflammation and steatosis. Because of prolonged CXCL13/YAP/PD-L1 activation in pancreatic cancers, neighboring noncancerous cells, activated for proliferation and immune-protected, eventually transform and accelerate tumor progression. CXCL13 blockade removed senescent cells and ameliorated steatosis in the aged pancreas while suppressing tumor growth in pancreatic cancer models, highlighting the CXCL13/YAP/PD-L1 axis as a potential therapeutic target. Together, our findings demonstrate the stress-induced CXCL13/YAP/PD-L1 axis as a central regulator of cell-state transitions in the pancreas, providing a unifying principle by which organ homeostasis, aging, and tumorigenesis are governed.

INTRODUCTION

Excessive stress causes cell senescence that irreversibly arrests the cell cycle. In addition, senescent cells display the senescence-associated secretory phenotype (SASP) and secrete paracrine signals to neighboring cells (*1*–*3*). We previously reported the conditional knockout of *Pdx1*, a pivotal transcription factor for pancreatic organogenesis (*4*, *5*), in adult acinar cells using *Elastase-CreER; Pdx1$^{floxed/floxed}$; Rosa-LacZ* mice (*Pdx1* cKO mice) (*6*). Upon tamoxifen (TAM) injection, a subset of Pdx1$^-$ acinar cells showed signs of mitochondrial stress and senescence. In contrast, neighboring Pdx1$^+$ acinar cells became proliferative to maintain organ size, indicative of the contribution of SASP in maintaining organ homeostasis in these *Pdx1* cKO mice.

Senescent cells are usually removed from organs by immunosurveillance. However, recent reports have shown that senescent cells accumulate in aged organs, with their removal shown to restore organ function (*7*–*12*), thus demonstrating the undesired effects of senescent cells and/or SASP during aging. In cancer biology, however, there has been a long-standing debate over the roles of cell senescence and SASP, induced regularly by chemo- or radiation therapy (*13*–*15*), as either anti- or pro-tumorigenic. Here, we identified CXCL13/YAP as the common core SASP signal orchestrating organ homeostasis after cellular stress, the accumulation of senescent cells and chronic inflammation during aging, as well as the progression of pancreatic cancer.

RESULTS

Stress-induced CXCL13/YAP activation stimulates compensatory proliferation of surrounding normal cells in the *Pdx1* cKO pancreas

We first performed a transcriptomic analysis to identify potential SASP-related molecules in the *Pdx1* cKO pancreas. *Cxcl13* (*16*, *17*) was identified as the top gene among up-regulated genes in *Pdx1* cKO pancreata compared to wild type (WT) (table S1). Histologically, CXCL13 was expressed exclusively in Pdx1-depleted acinar cells (Fig. 1A). Furthermore, we found activation of the Hippo-YAP pathway (*18*, *19*), normally observed in pancreatic ducts but not in acinar cells, exclusively in surrounding Pdx1$^+$ acinar cells. *Cxcl13* expression, as well as numbers of YAP$^+$ acinar and proliferating (pHH3$^+$) cells, were all transiently elevated and then decreased between 1 and 3 months after TAM injection and accompanied by the disappearance of p21$^+$ senescent and mitochondrial stressed cells in *Pdx1* cKO mice (Fig. 1, B and C). We next examined for similar changes in a model of acute mitochondrial stress in acinar cells [as reported previously in rats (*20*)] by injecting L-lysine (Lys) into WT mice (fig. S1A). We observed abnormal mitochondria at 24 hours after treatment, followed by mitophagy at 48 hours, with mitochondria appearing normal 1 week after injection. Some acinar cells became senescent, as evidenced by induced expression of *Cdkn2a* (encoding p16^{INK4a}) and senescence-associated β-galactosidase (SA-β-Gal) by 24 hours. In

[1]Division of Hepato-Biliary-Pancreatic Surgery and Transplantation, Department of Surgery, Graduate School of Medicine, Kyoto University, Kyoto, Japan. [2]Department of Life Science Frontiers, Center for iPS Cell Research and Application (CiRA), Kyoto University, Kyoto, Japan. [3]Department of Cell Growth and Differentiation, Center for iPS Cell Research and Application (CiRA), Kyoto University, Kyoto, Japan. [4]Department of Anatomy and Embryology, Faculty of Veterinary Medicine, Benha University, Toukh, Egypt. [5]Department of Anatomy and Embryology, Faculty of Veterinary Medicine, Damanhour University, Damanhour, Egypt. [6]Institute for the Advanced Study of Human Biology (ASHBi), Kyoto University, Kyoto, Japan. [7]Medical-risk Avoidance based on iPS Cells Team, RIKEN Center for Advanced Intelligence Project (AIP), Kyoto, Japan. [8]Department of Molecular Pathology, Graduate School of Medicine, The University of Tokyo, Tokyo, Japan. [9]Department of Drug Discovery Medicine, Kyoto University Graduate School of Medicine, Kyoto, Japan. [10]Foundation for Biomedical Research and Innovation at Kobe, Kobe, Japan. [11]Cold Spring Harbor Laboratory, Cold Spring Harbor, NY, USA. [12]Shiga University of Medical Science, Shiga, Japan.
*Corresponding author. Email: yoshiyak@cira.kyoto-u.ac.jp

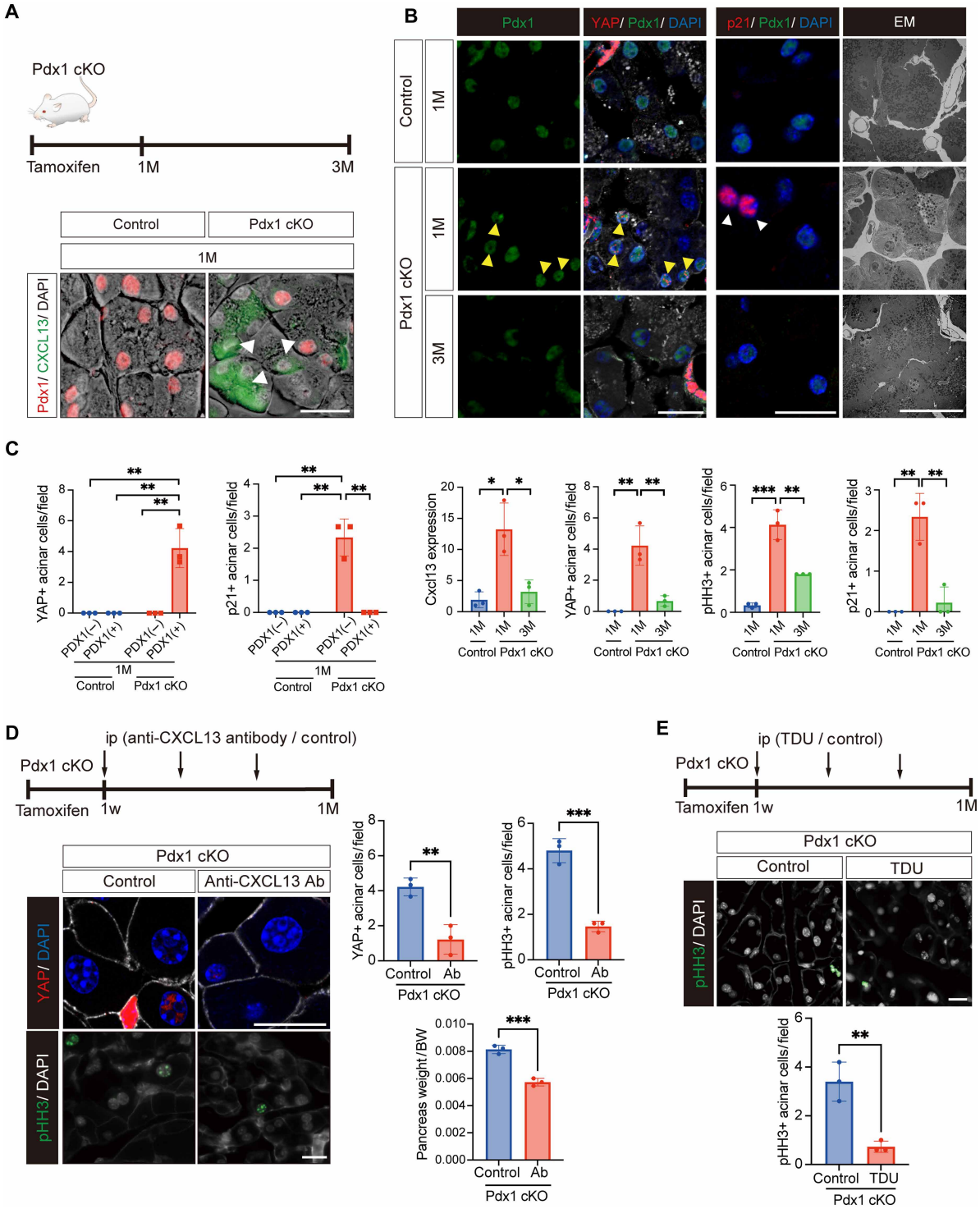

Fig. 1. Transient activation of stress-induced CXCL13-YAP signals maintained pancreatic homeostasis in *Pdx1* cKO mice. (**A** to **C**) Transient CXCL13/YAP activation and disappearance of stressed cells in *Pdx1* cKO mice. (A) Schematic diagram of *Elastase-CreER*–mediated *Pdx1* inactivation and CXCL13 expression in Pdx1$^-$ acinar cells (white arrowheads) at 1 month after TAM injection. (B) YAP and p21 expression and electron micrographs (EM). YAP$^+$ cells and p21$^+$ cells are exclusively detected in Pdx1$^+$ (yellow arrowheads) and Pdx1$^-$ (white arrowheads) cells at 1 month after TAM injection, respectively. (C) Numbers of YAP$^+$, pHH3$^+$, and p21$^+$ acinar cells ($n = 3$ for each group). *Cxcl13* expression ($n = 3$ in control, *Pdx1* cKO 1M, and *Pdx1* cKO 3M). 1M, 1 month; 3M, 3 months. (**D**) Anti-CXCL13 antibody (Ab) reduced the numbers of YAP$^+$ and PHH3$^+$ cells, as well as pancreas weight. ip, intraperitoneally; 1w, 1 week; BW, body weight. (**E**) YAP inhibition by Super-TDU suppressed acinar cell proliferation. Scale bars, 20 μm. Bars represent means ± SD. *$P < 0.05$; **$P < 0.01$; ***$P < 0.001$.

these Lys-treated WT pancreata, we observed the same SASP signals being activated, albeit more transiently, that were induced in *Pdx1* cKO mice after TAM treatment—CXCL13 expression, nuclear YAP, and *Ctgf* expression, a downstream target of YAP signaling (*21*, *22*), were observed at 24 hours and all gradually returned to normal levels by 3 weeks. CXCR5 expression, the ligand-induced receptor for CXCL13, was observed as early as 24 hours after Lys treatment and peaked at 1 week, in parallel with enhanced cell proliferation. Moreover, both CXCR5 expression and cell proliferation returned to the basal level at 3 weeks. No fibrosis was observed during this recovery process, and organ size was macroscopically maintained.

Activation of the same SASP signal in two different models prompted us to examine the role of CXCL13/YAP signaling using *Pdx1* cKO mice. We found that injecting anti-CXCL13 antibody suppressed YAP activation and cell proliferation in surrounding Pdx1$^+$ acinar cells, resulting in reduced pancreas size (Fig. 1D). In addition, Super-TDU, a Hippo-YAP signaling inhibitor (*23*), suppressed acinar cell proliferation in *Pdx1* cKO pancreata (Fig. 1E). These findings indicate that, upon mitochondrial stress, a subset of acinar cells become senescent and secrete CXCL13, which acts on surrounding acinar cells to stimulate cell proliferation via YAP activation to maintain organ size.

To elucidate the molecular mechanism underlying stress-induced CXCL13 expression, we established an in vitro primary culture system using normal pancreatic tissue, which successfully recapitulated the in vivo Lys treatment that induced a marked increase in *Cxcl13* expression (fig. S2A). We found that *Cxcl13* induction was accompanied by up-regulated nuclear factor κB (NF-κB) signaling, consistent with a previous report of its role in CXCL13 regulation (*24*, *25*). As expected, treatment with BAY 11-7082, an NF-κB inhibitor, significantly suppressed *Cxcl13* expression. Consistently, primary cultured *Pdx1* cKO pancreata showed a significantly higher *Cxcl13* and NF-κB activity compared to WT, whereas BAY 11-7082 reduced *Cxcl13* expression (fig. S2B). These results indicate the involvement of NF-κB–dependent signaling, which induces *Cxcl13* expression in response to cellular stress in pancreatic acinar cells.

Next, we used rat acinar cell line AR42J, which is positive for *Pdx1* expression, to dissect the intracellular mechanism by which CXCL13 activates YAP to stimulate surrounding cells to proliferate. Recapitulating our findings in the surrounding Pdx1$^+$ acinar cells in *Pdx1* cKO mice, recombinant CXCL13 (rCXCL13) treatment induced YAP expression with increased *Ctgf* expression and stimulated proliferation (fig. S3A). However, YAP activation was suppressed by the G_i inhibitor pertussis toxin (PTx) (*26*) and treatment with either PTx or Super-TDU decreased cell proliferation. Because CXCR5 is a $G\alpha_i$-coupled receptor, these results indicate that CXCL13-CXCR5 signaling activates YAP through $G\alpha_i$, which, in turn, stimulates proliferation. Furthermore, we investigated why YAP was not activated in Pdx1$^-$ cells in *Pdx1* cKO pancreata. To address this question, we knocked down *Pdx1* expression using short hairpin RNA (shRNA) in AR42J cells. Stimulation with XMU-MAP-1, a selective inhibitor of MST1/2 kinase, activates YAP signaling in shControl-treated, normal AR42J cells. However, YAP fails to translocate to the nucleus in *Pdx1* knockdown cells, indicating that Pdx1 is required for YAP activation in acinar cells (fig. S3B).

CXCL13-driven autocrine anti-apoptotic signaling and PD-L1–mediated immune escape protect stressed acinar cells in *Pdx1* cKO mice

Transient CXCL13/YAP axis activation, followed by the disappearance of stressed cells in both the *Pdx1* cKO and Lys injection models, indicates that a common mechanism must exist to preserve stressed cells until the completion of compensatory proliferation. We noticed that, upon TAM treatment, CXCR5 expression and pERK activation were transiently induced not only in surrounding Pdx1$^+$ cells but also in stressed Pdx1$^-$ cells in *Pdx1* cKO mice (Fig. 2, A and B). Notably, injecting anti-CXCL13 antibody, but not Super-TDU, resulted in caspase-3 activation (predominantly in Pdx1$^-$ cells) and a reduction of p21$^+$ cells (Fig. 2, C and D). Consistently, lineage-labeled cells in *Elastase-CreER; Pdx1$^{loxP/loxP}$; ROSA-LacZ* mice, which represent *Pdx1*-depleted, stressed cells, were decreased by anti-CXCL13 antibody injection (Fig. 2E). Furthermore, we established a Lys-induced stress model using AR42J cells. Notably, whereas our apoptosis assay revealed that the percentage of Caspase-3/7–expressing cells was comparable between the rCXCL13-treated samples and those co-treated with Super-TDU, apoptotic cells were significantly increased by PTx or U0126, a MEK inhibitor (fig. S4A). These findings indicate that distinct signaling pathways—ERK/MAPK- and YAP-dependent pathways, respectively—mediate the autocrine anti-apoptotic and paracrine proliferative effects of CXCL13 in stressed cells and surrounding cells (see fig. S3A).

In addition, we observed the transient expression of PD-L1, a ligand for the inhibitory checkpoint molecule PD-1 (*27*, *28*), accompanied by transient infiltration of CD45$^+$ immune cells in *Pdx1* cKO mice (Fig. 2F). PD-L1 expression in *Pdx1* cKO mice was detected both in Pdx1$^+$ and Pdx1$^-$ acinar cells at 1 month but disappeared predominantly in Pdx1$^-$ cells 3 months after TAM injection. Likewise, we observed transient PD-L1 expression and immune cell infiltration after Lys injection in WT pancreata (fig. S1B). The number of CD45$^+$ immune cells was reduced by injecting anti-CXCL13 antibody, but not by Super-TDU, in *Pdx1* cKO mice, reflecting properties of CXCL13 as an immune cell attractant (Fig. 2G) (*16*). Notably, injecting either anti-CXCL13 antibody or Super-TDU treatment decreased PD-L1 expression in Pdx1$^+$ cells, but PD-L1 suppression was not significant in Pdx1$^-$ cells, indicating that PD-L1 expression is regulated via distinct mechanisms in Pdx1$^-$ and Pdx1$^+$ cells. Namely, whereas stress-induced PD-L1 expression in Pdx1$^-$ cells is CXCL13 independent, PD-L1 induction in surrounding Pdx1$^+$ cells depends on the CXCL13/YAP-mediated SASP signal (CXCL13/YAP/PD-L1 axis) (see Discussion). Our in vitro experiments using AR42J supported the existence of the CXCL13/YAP/PD-L1 axis in Pdx1$^+$ cells as rCXCL13 activated YAP and increased PD-L1 expression, but Super-TDU treatment canceled this PD-L1 elevation (fig. S4B).

Fluorescence-activated cell sorting (FACS) analyses of infiltrating immune cells in the *Pdx1* cKO pancreata 1 month after TAM injection revealed that multiple CD45+ subsets increased (~4.0 to 6.8% in control pancreata versus ~10.8 to 14.4% in *Pdx1* cKO pancreata, $n = 3$ for each group), including B cells, macrophages, neutrophils, and dendritic cells (fig. S5). Notably, B cells and macrophages in *Pdx1* cKO pancreata exhibited a significant up-regulation of PD-1 (Fig. 2H and fig. S5), and anti–PD-L1 antibody treatment reduced senescent cells (Fig. 2I). Thus, PDL-1 induction functions to preserve stressed cells by facilitating the escape from immune surveillance by PD-1$^+$ immune cells.

Together, these findings suggest an exquisite mechanism to preserve stressed cells until the completion of tissue restoration. Stress-induced CXCL13 exerts an autocrine effect to suppress apoptosis of stressed cells through CXCR5/MAPK-mediated signaling, independent of YAP. In addition, although immune cells with increased PD-1 expression infiltrate the stressed pancreas, PD-L1 induction

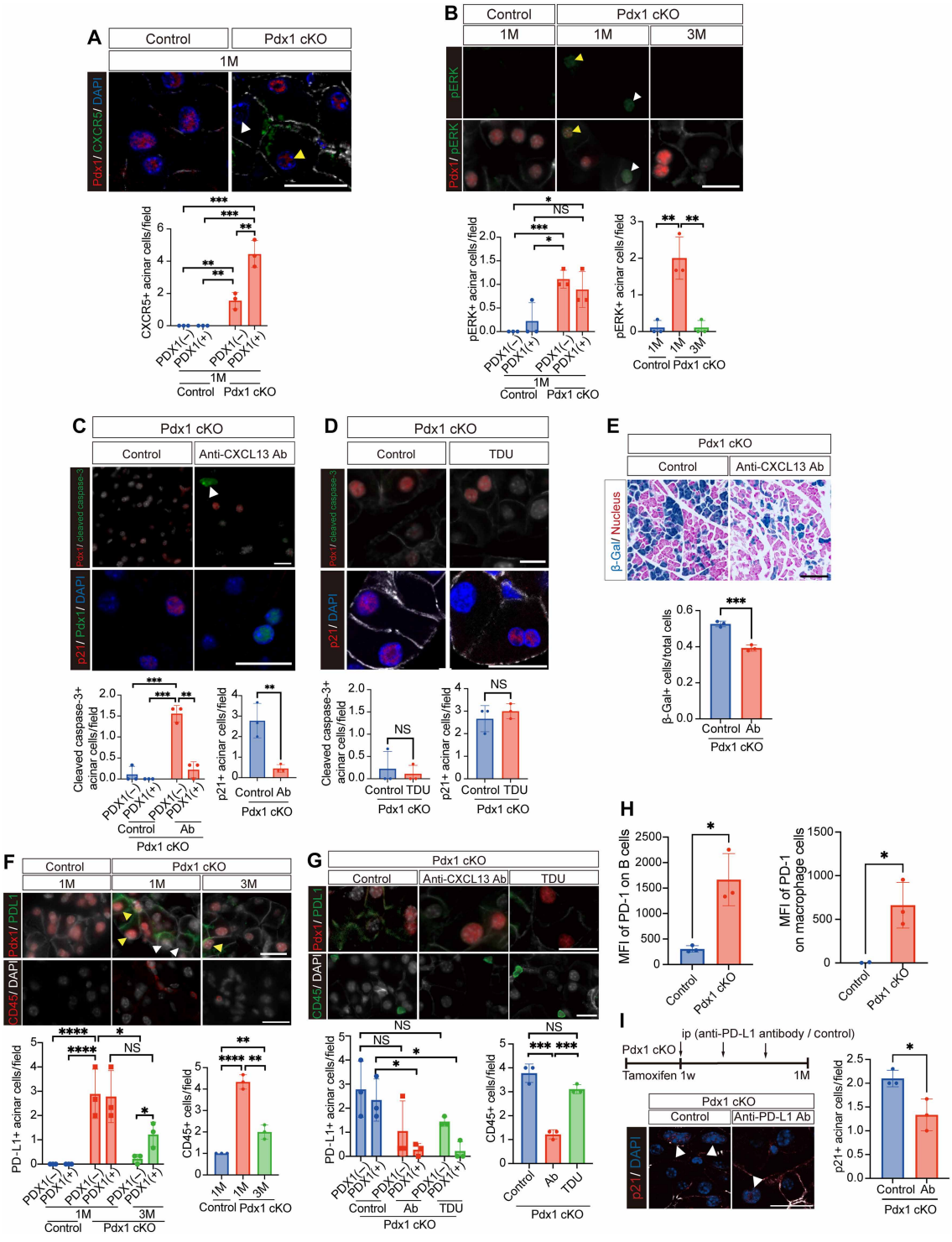

Fig. 2. Anti-apoptotic effect of CXCL13 on stressed cells and PD-L1–mediated immune evasion in *Pdx1* cKO pancreata. (**A**) Expression of CXCR5 in both Pdx1$^+$ (yellow arrowhead) and Pdx1$^-$ (white arrowhead) cells ($n = 3$ for each group). (**B**) Transient pERK activation in Pdx1$^+$ (yellow arrowhead) and Pdx1$^-$ (white arrowhead) cells ($n = 3$ for each group). (**C** to **E**) Anti-apoptotic effect of CXCL13. Anti-CXCL13 antibody induced apoptosis in Pdx1$^-$ cells (white arrowhead) and reduced the number of p21$^+$ senescent cells ($n = 3$ for each group), but Super-TDU did not ($n = 3$ for each group). The number of lineage-labeled cells (*Pdx1*-depleted cells) was reduced ($n = 3$ for each group). (**F** to **I**) PD-L1–mediated immune evasion. PD-L1 is induced in both Pdx1$^+$ (yellow arrowheads) and Pdx1$^-$ (white arrowheads) cells, accompanied by transient infiltration of CD45$^+$ immune cells ($n = 3$ for each group). PD-L1 expression was reduced by either anti-CXCL13 antibody or Super-TDU in Pdx1$^+$ cells, whereas infiltration of CD45$^+$ cells was suppressed by anti-CXCL13 antibody but not by Super-TDU (n = 3 for each group). FACS analyses revealed that infiltrated B cells and macrophages express higher PD-1 ($n = 3$ for each group). Anti-PDL-1 antibody injection reduced the number of senescent cells ($n = 3$ for each group). Scale bars, 20 μm. Bars represent means ± SD. NS, not significant; *$P < 0.05$; **$P < 0.01$; ***$P < 0.001$; ****$P < 0.0001$.

in pancreatic cells promotes a suppressive environment for immune surveillance.

CXCL13 blockade reduced senescent cells and ameliorated chronic inflammation and pancreatic steatosis in aged animals

Consistent with previous reports of increased senescent cells and chronic inflammation in aged organs (*9*, *29*–*31*), we observed increases in $p21^+$ senescent acinar cells and immune cell infiltration in the aged pancreas compared to the young organ. Notably, immunohistochemical staining revealed increased expression of CXCL13, YAP, and PD-L1 in aged acinar cells, rarely seen in normal acinar cells of young mice (Fig. 3A). Quantitative polymerase chain reaction (qPCR) analyses confirmed significant increases in the expression of *Cxcl13* and *Pdl1*. Similar to findings in *Pdx1* cKO mice, anti-CXCL13 antibody injection caused accelerated apoptosis, resulting in reductions of $p21^+$ senescent cells and infiltrating immune cells (Fig. 3B). Ultimately, CXCL13 blockade significantly ameliorated pancreatic steatosis, which is reported to advance in aged human and rodents (*32*–*34*) (Fig. 3C), thus highlighting the pivotal role of CXCL13 in pancreatic aging.

Prolonged activation of the CXCL13/YAP/PD-L1 axis in pancreatic cancer

Considering that the incidence of pancreatic cancer increases in aged individuals whose pancreas contains more stressed cells and undergoes chronic inflammation, our findings prompted us to examine the effects of CXCL13-mediated SASP signaling in pancreatic cancers. We first created mice with a conditional *Pdx1* deletion in oncogenic acinar cells [*Elastase-CreER; LSL-Kras*^{G12D}*; LSL-Trp53*^{R172H}*; Pdx1*$^{floxed/floxed}$*; Rosa-LacZ* mice (EKP-*Pdx1* cKO)] (fig. S6A). In this mouse, TAM injection induces oncogenic $Kras^{G12D}$ and $p53^{R172H}$ expression concomitant with *Pdx1* deletion in a subpopulation of adult acinar cells, enabling us to distinguish the *Pdx1*-deleted oncogenic cells and normal cells as β-galactosidase $(β\text{-Gal})^+$ and $β\text{-Gal}^-$ cells, respectively. Consistent with our findings in *Pdx1* cKO mice (Fig. 1B) (*6*), *Pdx1* deletion led to enhanced cellular stress, as evidenced by round mitochondria with diminished cristae and endoplasmic reticulum (ER) with an enlarged lumen (fig. S6B), and cell senescence ($γH2AX^+$) (*35*, *36*) in a subset of *Pdx1*-depleted, namely, $β\text{-Gal}^+$ cells (fig. S6C).

Compared to *Elastase-CreER; LSL-Kras*^{G12D}*; LSL-Trp53*^{R172H}*; Rosa-LacZ* mice without *Pdx1* depletion (EKP-*Pdx1* WT mice), tumor sizes were significantly larger in EKP-*Pdx1* cKO mice 3 months after TAM injection (Fig. 4A and fig. S7A), with increased fibrosis, which has been postulated to function as a tumor niche (*37*). Transcriptomic analyses revealed that, in addition to *Cxcl13*, the expression of several cytokines [e.g., *interleukin-1*α (*Il-1*α) and *Il-1*β] and chemokines (e.g., *Ccl3*, *Ccl16*, and *Cxcl19*) was elevated 3 months after TAM injection in EKP-*Pdx1* cKO pancreata (table S2). These results indicate that severe inflammation was present in EKP-*Pdx1* cKO pancreata at this stage, leading to further immune cell infiltration and fibrosis. However, among the cytokines listed, only *Cxcl13* was highly expressed 2 months after TAM injection, before tissue fibrosis had manifested. CXCL13 was exclusively detected in *Pdx1*-depleted epithelial cells at 1 month after TAM injection and increased between 1 and 3 months (Fig. 4B), whereas CXCR5 expression was observed in both $Pdx1^-$ and $Pdx1^+$ acinar cells 3 months after TAM injection (fig. S7B). Notably, we detected nuclear YAP expression in both $Pdx1^-$ and $Pdx1^+$ acinar cells in EKP-*Pdx1* cKO pancreata 3 months after TAM injection (Fig. 4C), in sharp contrast to its exclusive expression in $Pdx1^+$ cells in *Pdx1* cKO mice at 1 month after TAM injection (see Fig. 1B). Correspondingly, YAP activity increased from 1 to 3 months after TAM injection, as evidenced by *Ctgf* expression. Likewise, although PD-L1 expression was only transient in *Pdx1* cKO pancreata, it extended from 1 to 3 months after TAM injection in EKP-*Pdx1* cKO pancreata (Fig. 4D). Furthermore, immune cell infiltration progressed from 1 to 3 months: We observed immune cells, including both CXCR5-expressing and CXCR5-negative $F4/80^+$ cells, $CD4^+$ cells, and $CD20^+$ cells, infiltrating the tumor in the latter stage when fibrosis was observed (fig. S8) (see Discussion). Together, these observations suggest dysregulated CXCL13/YAP signaling in pancreatic tumors due to *Pdx1* deletion.

Although cell proliferation was indistinguishable between $β\text{-Gal}^+$ and $β\text{-Gal}^-$ cells in EKP-*Pdx1* WT mice, it was significantly elevated in $β\text{-Gal}^-$ Pdx1-preserved cells in EKP-*Pdx1* cKO mice 3 months after TAM injection (Fig. 4E). Unexpectedly, cellular atypia [e.g., acinar-to-ductal metaplasia (ADM) and pathological carcinoma in situ (PanIN)] were observed in not only $β\text{-Gal}^+$ cells but also $β\text{-Gal}^-$ cells (Fig. 4F). With ~26.2 to 33.0% [30.4 ± 7.3(SD)] of $β\text{-Gal}^-$ normal cells classified as PanIN (fig. S9), normal acinar cells appear to have been induced to proliferate non-cell-autonomously and transformed by nearby oncogenic cells. To verify this hypothesis, we created chimeric mice by injecting *Elastase-CreER; LSL-Kras*^{G12D}*; LSL-Trp53*^{R172H}*; Pdx1*$^{floxed/floxed}$*; Rosa-LacZ* embryonic stem (ES) cells into enhanced green fluorescent protein (EGFP)–expressing blastocysts (Fig. 4G). In this chimeric mouse, cells undergoing oncogenic induction and *Pdx1* inactivation due to TAM injection are indicated by $EGFP^-$ $β\text{-Gal}^+$ cells, whereas $EGFP^+$ $β\text{-Gal}^-$ cells represent surrounding normal cells. Three months after TAM injection, non-cell-autonomously induced transformation was evidenced by $EGFP^+$ and lineage-negative ($β\text{-Gal}^-$) ADM and PanIN lesions in chimeric mice (Fig. 4H and fig. S10A). Consistently, CXCR5 expression was observed in both $EGFP^-$ and $EGFP^+$ cells 3 months after TAM injection (fig. S10B). Furthermore, ERK phosphorylation and YAP activation were observed in $EGFP^+$ cells (fig. S10, C and D).

We next injected Lys into EKP-*Pdx1* WT mice and found tumor progression to accelerate more aggressively than in EKP-*Pdx1* cKO mice without Lys treatment. PanIN lesions were detected at 3 weeks after Lys injection, with large tumors showing severe fibrosis detectable as early as 2 months after Lys injection (fig. S11A). Notably, Lys treatment caused prolonged cellular stress and CXCL13/YAP activation in EKP-*Pdx1* WT mice (fig. S11B) as SA-$β\text{-Gal}^+$ senescent cells with abnormal mitochondria and increased *Cdkn2a* expression were detected after 1 and 3 weeks. Furthermore, sustained CXCL13/YAP activation was indicated by increased expression of *Cxcl13* and *Ctgf*. We also observed sustained PD-L1 expression from 1 to 3 weeks, with increased immune cell infiltration at the latter time point (fig. S11C). These phenotypes contrasted greatly with those of normal mice, in which Lys treatment only produced transient phenotypic changes (see fig. S1).

To evaluate the relevance of our findings to human pancreatic cancers, we next examined the expression of CXCL13, p16, YAP, and PD-L1 in resected cancerous tissues (Fig. 5A). As expected, we confirmed their expression in human cancer samples and notably detected YAP and PD-L1 not only in ADM and PanIN but also in some phenotypically normal acinar cells adjacent to tumors, similar to our mouse data.

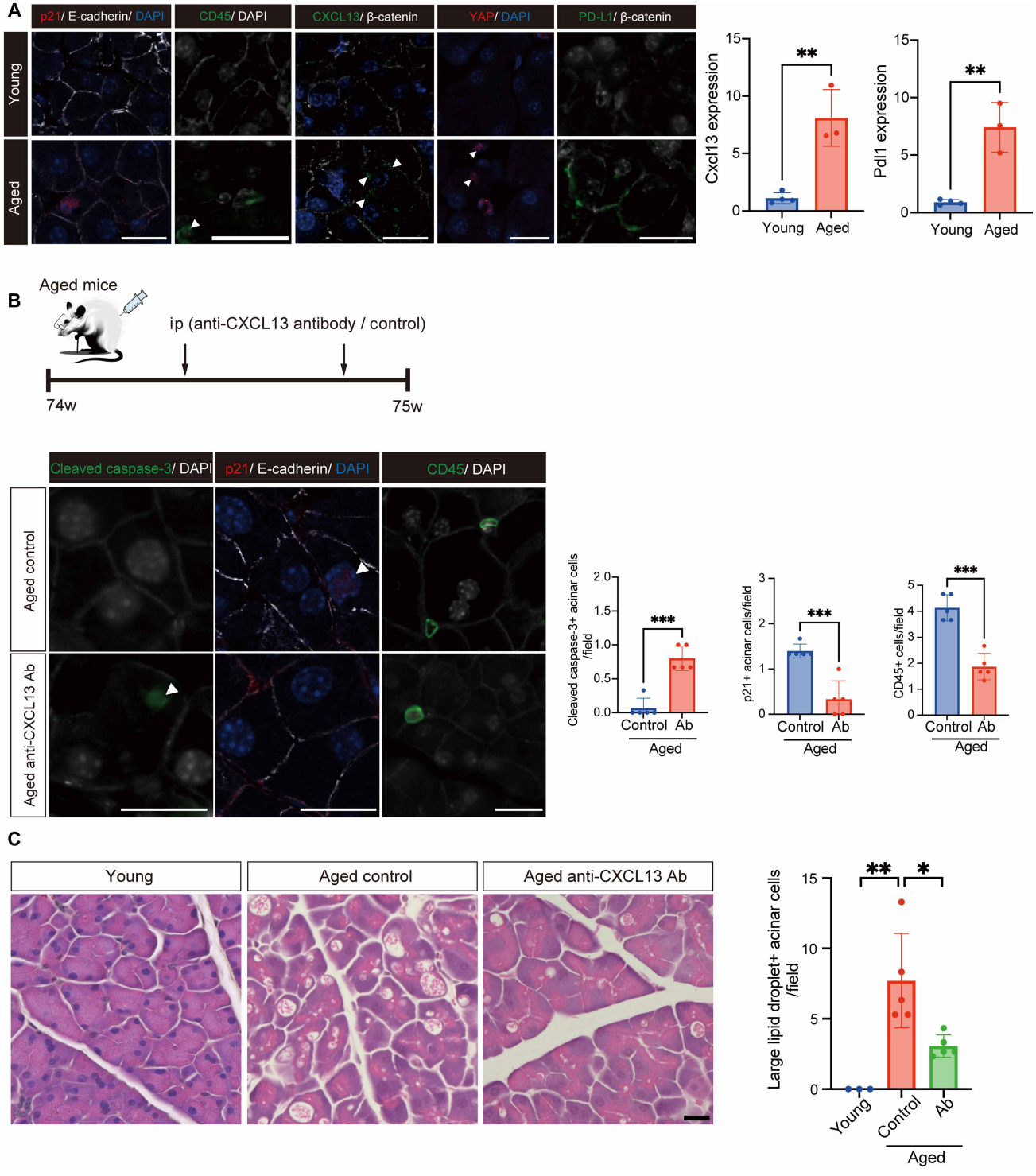

Fig. 3. Anti-CXCL13 antibody reduced senescent cells and ameliorated chronic inflammation and steatosis of the aged pancreas. (**A**) Accumulation of p21^{+} senescent cells, immune cell infiltration, and YAP/PD-L1 expression in the aged pancreas (young mice: 4 weeks and aged mice: 74 weeks). Higher expression of CXCL13 and PD-L1 was observed in the aged pancreas ($n = 4$ in young mice and $n = 3$ in aged mice). (**B**) Schematic diagram of CXCL13 injection in aged mice (74 weeks old). Anti-CXCL13 antibody increased the number of apoptotic cells with caspase-3 activation (white arrowhead) and reduced both the number of p21^{+} senescent cells (white arrowhead) and infiltrating CD45^{+} immune cells ($n = 5$ for each group). (**C**) Anti-CXCL13 antibody ameliorated pancreatic steatosis in aged mice. Note the reduction of large intra-acinar lipid accumulation (>10-μm lipid droplets) [$n = 3$ (young) and $n = 5$ (aged control and Ab)]. Scale bars, 20 μm. Bars represent means ± SD. *$P < 0.05$; **$P < 0.01$; ***$P < 0.001$.

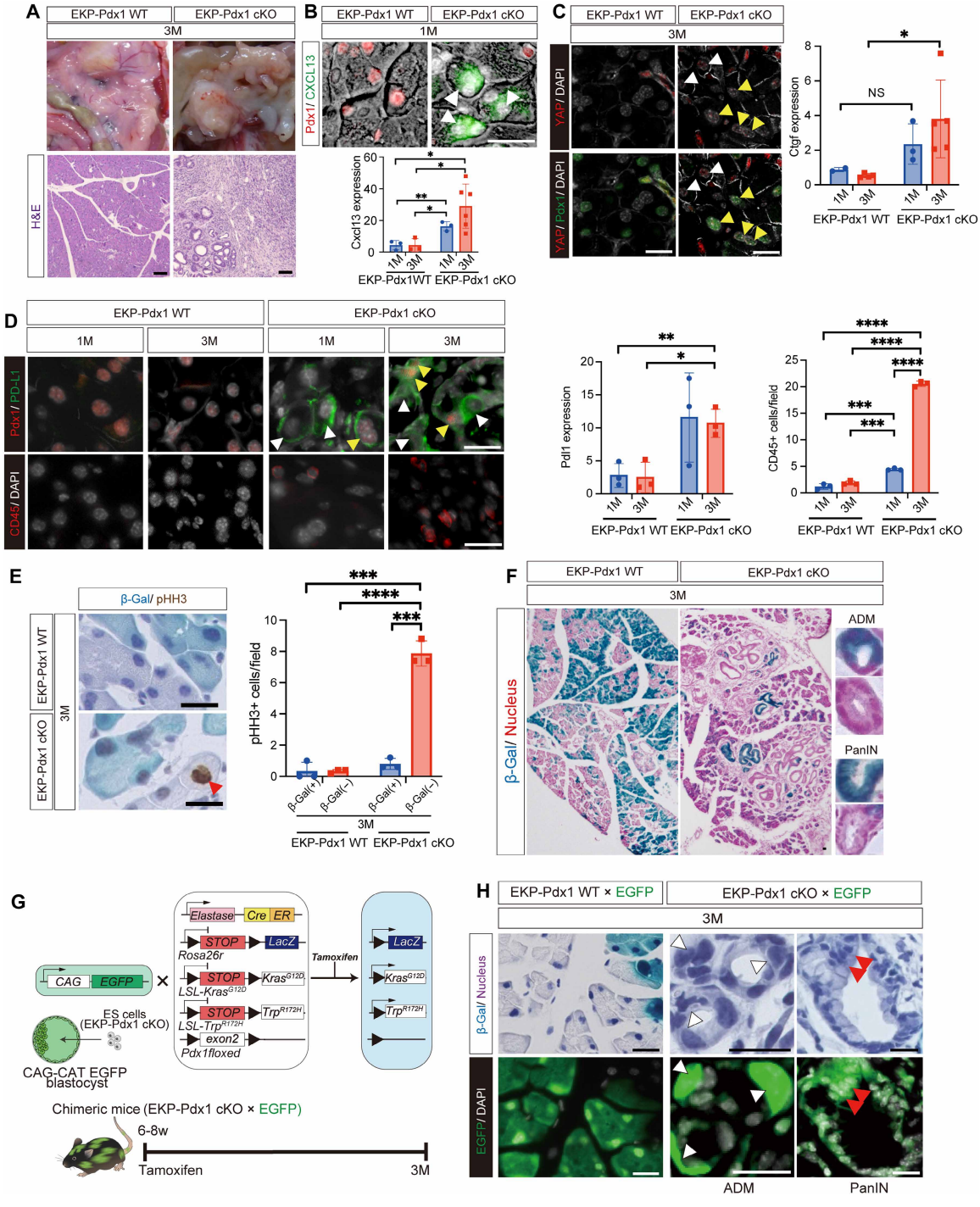

Fig. 4. *Pdx1* inactivation induced CXCL13-YAP signals and non-cell-autonomously promoted cancer progression in the pancreas. (**A**) Macroscopic and histological images showing accelerated tumor formation and fibrosis in EKP-*Pdx1* cKO pancreata at 3 months after TAM injection. H&E, hematoxylin and eosin. (**B**) Sustained CXCL13 expression in Pdx1$^-$ acinar cells (white arrowheads). *Cxcl13* expression [$n = 3$ (1M) and $n = 3$ (3M) for EKP-*Pdx1* WT mice; $n = 3$ (1M) and $n = 6$ (3M) for EKP-*Pdx1* cKO]. (**C**) Prolonged activation of Hippo-YAP signaling. Nuclear YAP expression in Pdx1$^+$ (yellow arrowheads) and Pdx1$^-$ (white arrowheads) acinar cells (left). *Ctgf* expression was elevated at 3 months after TAM injection [$n = 2$ (1M) and $n = 4$ (3M) for EKP-*Pdx1* WT mice; $n = 3$ (1M) and $n = 5$ (3M) for EKP-*Pdx1* cKO]. (**D**) Sustained PD-L1 expression and accelerated immune cell infiltration. Note the PD-L1 expression in both Pdx1$^-$ (white arrowheads) and Pdx1$^+$ (yellow arrowheads) acinar cells [$n = 3$ (1M) and $n = 3$ (3M) for EKP-*Pdx1* WT mice; $n = 3$ (1M) and $n = 3$ (3M) for EKP-*Pdx1* cKO]. (**E** and **F**) Non-cell-autonomously activated proliferation and transformation. Lineage tracing analyses showed activated proliferation of β-Gal$^-$ cells (red arrowhead) [$n = 3$ (3M) for EKP-*Pdx1* WT mice; $n = 3$ (3M) for EKP-*Pdx1* cKO], as well as ADM and PanIN in both β-Gal$^+$ and β-Gal$^-$ cells. (**G** and **H**) Chimeric mice experiments. Schematic diagram and EGFP$^+$ ADM (white arrowheads) and PanIN (red arrowheads). Scale bars, 20 μm. Bars represent means ± SD. NS, not significant; *$P < 0.05$; **$P < 0.01$; ***$P < 0.001$; ****$P < 0.0001$.

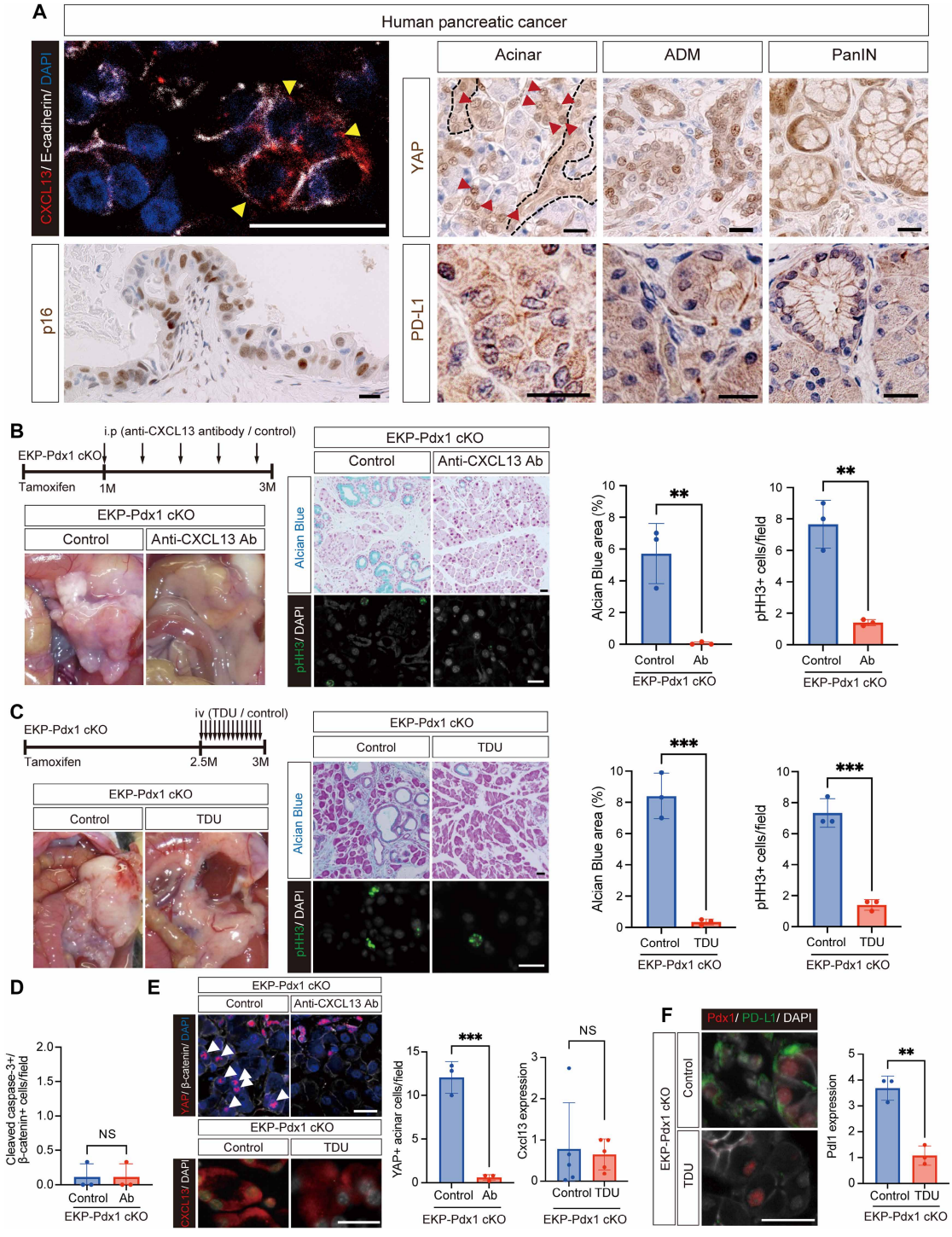

Fig. 5. Blocking the CXCL13/YAP axis suppressed tumor progression. (**A**) Expression of CXCL13, p16, YAP, and PD-L1 in resected human pancreatic cancer. CXCL13 expression in phenotypically normal acinar cells (yellow arrowheads). Note the restricted p16 expression in PanIN and YAP expression in phenotypically normal acinar cells (red arrowheads) near the tumor. (**B**) Anti-CXCL13 antibody suppressed tumor progression in EKP-*Pdx1* cKO mice. Experimental design and macroscopic view at 3 months after TAM injection. Histological analyses and quantification with Alcian Blue and pHH3 staining ($n = 3$ for both groups). (**C**) Inhibition of YAP signaling using Super-TDU suppressed tumor progression in EKP-*Pdx1* cKO mice. Experimental design and macroscopic view at 3 months after TAM injection. Histological analyses and quantification with Alcian Blue and pHH3 staining ($n = 3$ for both groups). iv, intravenously. (**D**) Anti-CXCL13 antibody treatment did not induce apoptosis in cancer. (**E**) Hippo-YAP signaling functions downstream of a CXCL13-mediated paracrine signal. Blocking CXCL13 attenuated YAP expression ($n = 3$ for each group), whereas Super-TDU did not affect *Cxcl13* expression in EKP-*Pdx1* cKO pancreata ($n = 5$ for each group). White arrowheads indicate enhanced YAP expression in acinar cells. (**F**) Super-TDU injection suppresses PD-L1 expression. Histological view and qPCR analyses ($n = 3$ for both groups). Scale bars, 20 μm. Bars represent means ± SD. NS, not significant; $^{**}P < 0.01$; $^{***}P < 0.001$.

CXCL13/YAP inhibition blocks cancer progression

Last, we examined the roles of CXCL13 and YAP in pancreatic cancer progression. We found that injecting anti-CXCL13 antibody or Super-TDU almost completely blocked tumor progression in EKP-*Pdx1* cKO mice and Lys-treated EKP-*Pdx1* WT mice (Fig. 5, B and C, and fig. S12, A and B). Specifically, Alcian Blue^{+} atypical cells were reduced, and cell proliferation and tissue fibrosis were significantly suppressed with either antibody or inhibitor treatment. Although CXCL13 showed an anti-apoptotic effect on stressed cells when maintaining organ size or in the aged pancreas (see Figs. 2C and 3B), we did not detect any apoptosis in response to anti-CXCL13 antibody treatment in EKP-*Pdx1* cKO cancers (Fig. 5D). In both EKP-*Pdx1* cKO mice and Lys-treated EKP-*Pdx1* WT mice, whereas CXCL13 expression was not affected by Super-TDU, anti-CXCL13 antibody reduced the number of YAP^{+} acinar cells in both models (Fig. 5E and fig. S12, C and D). These results demonstrate that the Hippo-YAP pathway functions downstream of CXCL13 signaling for pancreatic cancer progression. Consistently, PD-L1 expression was diminished by Super-TDU injection in EKP-*Pdx1* cKO mice (Fig. 5F). Thus, we conclude that stress-triggered CXCL13/YAP/PD-L1 signaling functions as a core mechanism that pancreatic tumors leverage for malignant growth.

DISCUSSION

We identified CXCL13 as the common signal activated by cellular stresses and CXCL13-mediated SASP to be responsible for normal physiological pancreatic homeostasis, chronic inflammation of the aged organ, and pancreatic cancer growth (Fig. 6). To maintain physiological homeostasis, the stress-induced CXCL13/YAP/PD-L1 axis gradually subsides with the concomitant removal of stressed cells. Mild and transient inflammation is localized and tightly controlled, evidenced by modest immune cell infiltration only. Accordingly, no fibrosis is apparent during tissue recovery. The anti-apoptotic effect of CXCL13 on stressed cells and PD-L1–mediated evasion from immunosurveillance entails an innate mechanism that allows them to survive and sustain the CXCL13/YAP/PD-L1 axis until tissue restoration is complete.

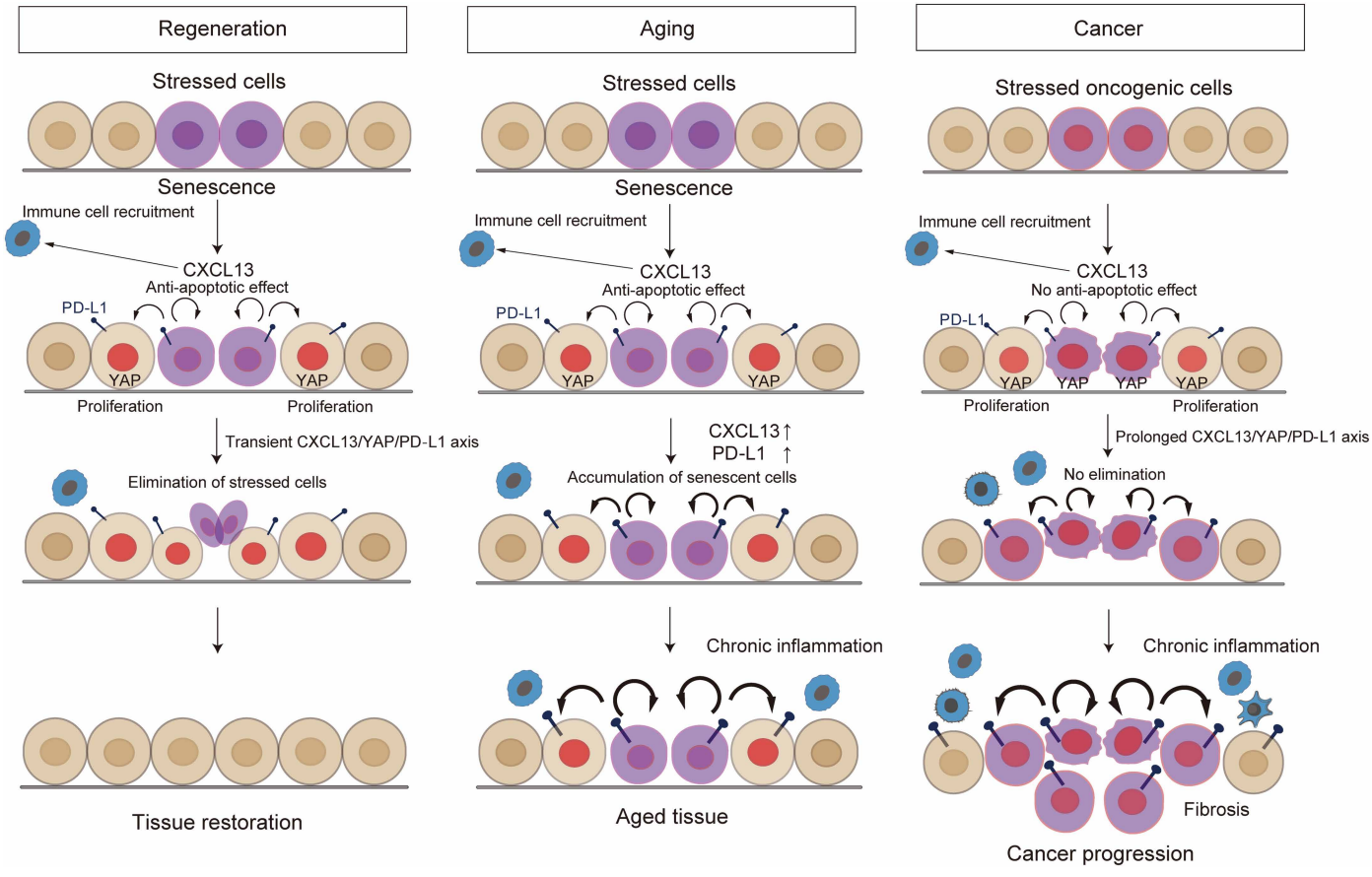

Fig. 6. Role of stress-induced CXCL13 in pancreatic exocrine homeostasis, chronic inflammation of the aged organ, and pancreatic cancer progression. Under normal physiological conditions, transient activation of the CXCL13/YAP/PD-L1 axis contributes to the maintenance of organ homeostasis. The anti-apoptotic effect of CXCL13 and PD-L1 expression promote the survival of stressed cells. As tissue restoration completes, stressed cells are removed from the organ, thus ending CXCL13/YAP/PD-L1 activation. Critically, immune cell recruitment by CXCL13 is mild and transient. In the aged organ, repeated stress and/or insufficient recovery from stress may sustain the elevated expression of CXCL13/PD-L1, leading to the accumulation of senescent cells and chronic inflammation. By contrast, CXCL13 does not have the same anti-apoptotic effect on stressed cancer cells, allowing stressed cells to survive longer and prolonging the activation of the CXCL13/YAP/PD-L1 axis, ultimately leading to the proliferation and transformation of surrounding cells, accompanied by chronic inflammation and tissue fibrosis. Note the YAP activation in both stressed cells and surrounding cells in cancer, which might inhibit competition-based cell elimination machinery due to differential YAP activities.

By contrast, stressed cells accumulate in aged pancreas and cancers, and persistent CXCL13 secretion recruits large numbers of immune cells, ultimately leading to chronic inflammation. Specifically, cancers appear to use this innate mechanism for their own survival and progression: When cells with activated oncogenes are stressed, they also secrete CXCL13, but for longer durations, such that surrounding normal cells are induced to proliferate and later transform into ADM and PanIN via YAP activation. Meanwhile, PD-L1 expression is maintained in both stressed cells and neighboring cells, allowing both to survive, with the former cells continuing to secrete CXCL13 to sustain feedforward CXCL13/YAP/PD-L1 signaling. Notably, cancer cells do not depend on CXCL13's anti-apoptotic effect, likely due to their already-disrupted apoptotic regulation. We believe that prolonged CXCL13/YAP/PD-L1 signaling triggers severe inflammation resulting in the formation of a tumor niche where immune cells beyond $CXCR5^+$ cells are recruited, presumably by enhanced immune cell–recruiting chemokines [e.g., CCL3, CCL17, and CXCL16 (*38*, *39*)]. Furthermore, induction of pro-inflammatory and pro-tumorigenic cytokines [e.g., IL-1α and IL-1β (*39*, *40*)] at this stage would be involved in the proliferation and transformation of surrounding normal cells, as well as tissue fibrosis.

What determines the duration of stressed cell persistence in the normal pancreas? Considering our finding that stress-induced NF-κB activity regulates CXCL13 expression in pancreatic acinar cells and the roles of NF-κB in stress-induced responses in aging and cancers, including PD-L1 regulation (*41*, *42*), we speculate that stress strength, duration, or frequency determines CXCL13/PD-L1 expression via NF-κB activity, thereby controlling the duration of stressed cell survival. Upon transient stress in Lys-treated mice without oncogenic induction, transient expression of CXCL13 and PD-L1, both of which are likely regulated by NF-κB signaling (fig. S2) (*41*, *43*), alone would be unable to sustain stress cells for an extended period. Conversely, continuous or repetitive stress in the aged organ elevates NF-κB (*42*), thus maintaining CXCL13/PD-L1 expression and leading to the persistence of stressed cells. By contrast, in cancers, given that prolonged activation of the CXCL13/YAP/PD-L1 axis continues even after transient stress, as evidenced by Lys injection experiments, activated oncogenes may be responsible for extended CXCL13/PD-L1 expression, which allows stressed cells in cancers to survive or evade the immune system for long durations. Moreover, although YAP was activated in both stressed cells and surrounding cells in pancreatic cancers, it was detected in surrounding acinar cells but not in stressed acinar cells under normal physiological homeostasis, as evidenced in *Pdx1* cKO pancreata. As cell competition is known to occur among cells with different YAP activities, cells with high YAP activity survive as "winners," whereas YAP^{low} cells are eliminated as "losers" (*44*). Thus, stressed cells would be eliminated as "losers" in the normal pancreas, but such competition-based cell elimination machinery is likely inactive in cancers.

Consistently, we also documented the expression of CXCL13, p16, YAP, and PD-L1 in human pancreatic cancer samples and, more notably, found that treatments with anti-CXCL13 antibody or YAP inhibitor markedly suppressed tumor progression in our pancreatic cancer model. These results demonstrate the biological significance of the CXCL13/YAP/PD-L1 axis not only in pancreatic cancer development but also as a potential therapeutic target. In addition, we demonstrated that anti-CXCL13 antibody treatment significantly reduced stressed cells and ameliorated chronic inflammation, ultimately reversing pancreatic steatosis in the aged organ. Considering the accumulating evidence showing the favorable effects of senolytics on the functions of aged organs and the undesirable effects of SASP in cancers, as shown in this study, further mechanistic examination and its clinical application could lead to a markedly improved outcome for pancreatic cancer and senescence-associated diseases.

MATERIALS AND METHODS

Mice

ElastaseCre-ERTM (*45*), *LSL-Kras*^{G12D}, *LSL-Trp53*^{R172H}, *Pdx1 floxed,* and *ROSA-LacZ* (*ROSA26r*) mice were described previously (*45*–*49*) and bred for experiments.

B6J-aged mice were obtained from JAX Japan. All animal experiments were performed in accordance with the Kyoto University guidelines for animal experiments and were approved by the animal research committee of Kyoto University (approval no. 20-138).

TAM injection

Four milligrams of TAM (T5648, Sigma-Aldrich) was injected intraperitoneally into mice (~6 to 8 weeks old).

Generation of chimeric mice

EGFP-expressing blastocysts were obtained from C57BL/6 female and *CAG-CAT-EGFP* [C57BL/6-Tg(*CAG-EGFP*)] (*50*) male mice by in vitro fertilization and injected with *Elastase-CreER; LSL-Kras*^{G12D}*; LSL-Trp53*^{R172H}*; Pdx1*$^{flox/flox}$*; ROSA-LacZ* ES cells under an OLYMPUS IX71 microscope as previously described (*51*). Chimeric mice in which the contribution of *Elastase-CreER; LSL-Kras*^{G12D}*; LSL-Trp53*^{R172H}*; Pdx1*$^{flox/flox}$*; ROSA-LacZ* ES cells was more than 50% were excluded from the analyses. Results were confirmed by at least five independent experiments, with representative data shown.

Histology, immunohistochemistry, and immunofluorescence

Tissue preparation, immunohistochemistry, and immunofluorescence were performed as described previously (*52, 53*), and images were taken using an HS All-in-one Fluorescence Microscope BZ-9000E, BZ-X810 (Keyence), and Zeiss LSM700 and LSM900 (Carl Zeiss) microscopes. Primary and secondary antibodies used are listed in tables S3 and S4. Tissue preparation was performed with cardiac perfusion fixation with fixation solution [0.1 M phosphate buffer containing 2 mM $MgCl_2$, 5 mM EGTA, 4% paraformaldehyde (PFA), 2% glutaraldehyde (GA), and 30% sucrose], and dissected specimens were embedded in O.C.T. compound (Sakura). For X-galactosidase (X-Gal) staining, frozen sections were cut into 4-μm-thick slices and reacted as previously reported. The immunofluorescence protocol was modified to detect CXCL13, in which an animal-free blocking reagent (Vector) was used as the blocking solution, followed by incubation with the primary antibody diluted in the animal-free blocking solution at 4°C overnight. The secondary antibody was also diluted in the animal-free blocking solution. Alcian Blue and SA-β-Gal staining were performed using standard protocols. Briefly, for Alcian Blue staining, sections were immersed in 3% acetic acid and treated with Alcian Blue Stain Solution (pH 2.5; Muto Pure Chemicals) for 60 min. Sections were counterstained with a Contrast Red Solution (Funakoshi). SA-β-Gal staining was used to detect senescent cells in accordance with the manufacturer's protocol (Senescence Cells Histochemical Staining Kit, Sigma-Aldrich).

Electron microscopy

For tissue preparation, 4% PFA/2% GA in phosphate-buffered saline (PBS) was used as the perfusion solution. Specimens were cut into ~1-mm^3 volumes, immersed in the same solution overnight, post-fixed with osmium tetroxide, and prepared as ultrathin sections by uranium staining. Tissues were analyzed by a transmission electron microscope (H-7650, Hitachi) at the Division of Electron Microscopic Study (DEMS), Kyoto University.

RNA isolation and RT-PCR

RNA isolation and reverse transcription polymerase chain reaction (RT-PCR) were performed as described previously (*6*, *53*). Total RNA was extracted using the RNeasy Mini and Micro Kit (Qiagen), and cDNA was synthesized using the ReverTra Ace qPCR RT Master Mix (Toyobo), following the manufacturer's protocol. Primer sequences are listed in table S5.

Microarray analyses

The precise procedure was described previously (*54*). Briefly, 250 ng of total RNA was subjected to cDNA synthesis with a GeneChip WT Expression Kit (Ambion), and the resultant cDNA was fragmented and hybridized to a mouse Gene 1.0 ST Array (Affymetrix). Hybridized GeneChip arrays were washed and stained on a GeneChip Fluidics Station 450 (Affymetrix) and detected by a Scanner 3000 TG system (Affymetrix) according to the manufacturer's instructions. Microarray data were analyzed with GeneSpring GX14.9 software (Agilent Technologies).

In vivo anti-CXCL13 and anti–PD-L1 antibody treatment

Anti-CXCL13 neutralizing antibody (R&D, MAB470) or control immunoglobulin G (IgG) (R&D, MAB006) was injected intraperitoneally once every 10 days for a total of five treatments, at doses of 200, 200, 200, 150, and 150 μg per mouse in the cancer model. In the Lys model, treatments started 2 weeks after TAM injection. For the *Pdx1* cKO model, treatments began 1 week after TAM injection, and the antibody was injected intraperitoneally at 200 μg per mouse weekly. For the aged model, 200 μg per mouse was injected twice a week. Anti-mouse PD-L1 (#BE0101) or IgG2b control (#BE0090) was administered intraperitoneally at 300 μg per mouse once weekly for a total of three doses.

In vivo Super-TDU treatment

A dose (500 μg/kg) of Super-TDU (Selleck Chemicals) or control saline was injected by tail vein injection daily for 2 weeks in the cancer model. In the *Pdx1* cKO model, weekly intraperitoneal injections were started 1 week after TAM administration.

In vivo Lys treatment

Mice were injected intraperitoneally with Lys (1.6 g/kg; Tokyo Chemical Industry Co).

Cell culture

AR42J cells (American Type Culture Collection, CRL-1492) were maintained in Ham's F-12 K medium (Gibco) supplemented with 20% fetal bovine serum (FBS; Gibco), penicillin (100 U/ml), and streptomycin (100 μg/ml; Nacalai Tesque) and cultured at 37°C with 5% CO_2.

Primary pancreatic acinar cells were isolated from control and *Pdx1* cKO mice using a standard collagenase digestion protocol. Briefly, pancreata were minced, incubated in Liberase (200 μg/ml; Roche) at 37°C for 30 min and mechanically dissociated. Acinar clusters were washed and cultured in Dulbecco's modified Eagle's medium (DMEM; Gibco) supplemented with 10% FBS and 1% penicillin/streptomycin (P/S). After dissociation, primary acinar cells were plated at ~1×10^5 cells per well in 24-well plates (BD Falcon) and cultured for 1 day, followed by Lys-induced stress experiments on the next day.

In vitro stress induction by Lys

To induce cellular stress in vitro, Lys treatment was applied to primary cultured acinar cells and AR42J cells. Stock solutions (200 mM) of Lys were prepared in PBS (pH 7.4).

For primary cultured acinar cells, Lys was added to the culture medium at a final concentration of 40 mM, and cells were treated for 2 to 4 hours. NF-κB activity was inhibited using 10 μM BAY 11-7082 (TCI), with a 30-min pretreatment before Lys exposure.

For AR42J cells, cells were treated with 10 mM Lys for 6 hours to assess stress-induced apoptosis. For pharmacological pretreatments, AR42J cells were incubated on μ-Slide 8 Well chamber slides (ibidi) as follows: PTx (Merck, 100 ng/ml) for 12 hours, U0126 (Selleck Chemicals, 10 μM) or Super-TDU (Selleck Chemicals, 200 ng/ml) for 1 hour, and recombinant CXCL13 (rCXCL13; R&D Systems, 1 μg/ml) for 2 hours before Lys exposure. Lys treatment was performed in F-12 K medium supplemented with 2% FBS, and cells were analyzed 6 hours after treatment.

For apoptosis detection, CellEvent Caspase-3/7 Green Detection Reagent (Invitrogen) was added 1 hour before fixation. After a PBS wash, cells were fixed with 4% PFA for 15 min at room temperature, and nuclei were counterstained with 4′,6-diamidino-2-phenylindole (DAPI).

Effects of rCXCL13 on YAP modulation and cell proliferation

To examine the effect of rCXCL13 on YAP activity, AR42J cells were plated at low confluency (~30 to 40%) and subjected to 12 to 16 hours of serum starvation before stimulation. Recombinant CXCL13 (rCXCL13; 1 μg/ml) in serum-free F-12 K medium was added, and analyses were performed 2 hours after treatment. For RNA extraction, cells were cultured in 24-well plates, whereas μ-Slide 8 Well chamber slides (ibidi) were used for immunofluorescence. For PD-L1 analysis, cells were evaluated 8 hours after rCXCL13 treatment. Where indicated, Super-TDU was added 1 day before stimulation.

To evaluate the effect of rCXCL13 on cell proliferation, AR42J cells were seeded onto μ-Slide 8 Well chamber slides and treated with recombinant CXCL13 (1 μg/ml) in serum-free F-12 K medium, with PTx (100 ng/ml) and Super-TDU (200 ng/ml) added concurrently. After 24 hours, cells were rinsed with PBS, fixed with 4% PFA for 15 min at room temperature, and immunostained for Ki-67 to assess cell proliferation.

Effect of *Pdx1* knockdown on YAP nuclear localization

shRNA constructs targeting rat *Pdx1* (shrPdx1; VB250704) and a non-targeting control (shControl; VB010000) were purchased from VectorBuilder. AR42J cells were transfected with the indicated shRNAs using Lipofectamine 3000 (Thermo Fisher Scientific), according to the manufacturer's instructions. Where indicated, XMU-MP-1 (Selleck Chemicals; 3 μM) was added 1 day before analysis. Cells were analyzed 72 hours after shRNA transfection.

For YAP nuclear localization analysis, immunofluorescence images were acquired, and YAP nuclear localization was quantified from ≥10 selected fields and ≥20 cells per biological replicate. Data represent means ± SD from three independent experiments.

DSP-based preparation and dissociation of pancreatic samples for flow cytometry

A DSP stock solution was prepared by dissolving dithiobis(succinimidyl propionate) (DSP; Thermo Fisher Scientific) at 50 mg/ml in high-quality 100% anhydrous dimethyl sulfoxide (DMSO; Thermo Fisher Scientific). A working solution (1 mg/ml) was freshly prepared by diluting the stock solution in PBS immediately before use. Samples were treated with DSP at the indicated final concentration and incubated, and cross-linking was quenched with 1 M tris-HCl (Thermo Fisher Scientific) for 15 min at room temperature, followed by enzymatic dissociation using the Liberase Research Grade (200 μg/ml in PBS; Roche) at 37°C for 30 min. Cell suspensions were passed through a 70-μm pluriStrainer Mini cell strainer (pluriSelect) and washed with PBS containing 1% bovine serum albumin (BSA). Samples were cryopreserved in liquid nitrogen and subsequently used for flow cytometric analysis.

Flow cytometric analysis

Dispersed DSP-fixed single cells from mouse pancreas were stained with antibody mixtures listed in table S6 (BioLegend) in D-PBS(−) containing 2% FBS (Thermo Fisher Scientific) at 4°C overnight (~16 hours) after Fc receptor blocking using FcR Blocking Reagent, mouse (Miltenyi Biotec), according to the manufacturer's instructions. As the samples were prefixed, surface antigens were analyzed without viability dye staining or additional permeabilization. Data were acquired on a BD FACS Symphony A5 SE flow cytometer (BD Biosciences) using BD FACSDiva software (version 9.0.2) and analyzed with FlowJo software (version 10.10.0). Gating strategies for lymphoid and myeloid subsets are shown in fig. S5. Positivity for each antigen was defined using unstained controls, and the median fluorescence intensity (MFI) of PD-1 was calculated as the median PD-1 fluorescence intensity of the entire cell population in each fraction.

Statistical analyses were performed using JASP (version 0.94.5; University of Amsterdam, North Holland, The Netherlands). Comparisons between control and *Pdx1* cKO samples were conducted using the two-tailed Mann-Whitney *U* test. For reference, a two-tailed Welch's *t* test was also performed to confirm statistical significance. The frequency of CD45-positive cells, proportions of lineage subsets within the CD45-positive population, and the MFI of PD-1 were analyzed. For MFI-based analyses, only fractions in which more than 100 events were recorded were included. A P value of <0.05 was considered statistically significant.

Image quantification

Image quantification was performed on at least three nonoverlapping fields per sample, using three independent sections for each biological replicate. For cell proliferation, $pHH3^+$ cells were manually counted at 200× magnification in five fields. For the evaluation of Alcian $Blue^+$ and tumor areas, images acquired at 40× magnification from three fields were processed and analyzed using ImageJ software (NIH). For lineage tracing, $\beta\text{-}Gal^+$ and $\beta\text{-}Gal^-$ cells were manually counted at 200× magnification in five random sections per mouse. $\beta\text{-}Gal^+$ and $\beta\text{-}Gal^-$ PanIN cells were counted at 200× magnification in five fields.

Intranuclear YAP^+, $p21^+$, $CXCR5^+$, $pERK^+$, cleaved caspase-3^+, PD-$L1^+$, $CD45^+$, Ki-67^+, Caspase-$3/7^+$, and $DAPI^+$ cells were counted at 400× magnification in three fields. For steatosis analysis, large lipid droplet–positive (>10 μm) acinar cells were manually counted at 200× magnification in three fields.

Human samples

Pancreatic cancer specimens were collected from patients who underwent resection at the Kyoto University Hospital between January 2016 and November 2018. The study protocols were approved by the institutional review committee at Kyoto University (R0455) and met the guidelines of the responsible governmental agency.

Statistical analysis

All indices were analyzed using an unpaired Student's *t* test (two-tailed) or one-way analysis of variance (ANOVA) in Prism 10 (GraphPad), with differences yielding a P value of less than 0.05 deemed significant. The imaging data presented are representative images from more than three biologically independent experiments ($n > 3$).

Supplementary Materials

This PDF file includes:

Figs. S1 to S12
Tables S1 to S6

REFERENCES

1. M. Demaria, N. Ohtani, S. A. Youssef, F. Rodier, W. Toussaint, J. R. Mitchell, R. M. Laberge, J. Vijg, H. Van Steeg, M. E. Dollé, J. H. Hoeijmakers, A. de Bruin, E. Hara, J. Campisi, An essential role for senescent cells in optimal wound healing through secretion of PDGF-AA. *Dev. Cell* **31**, 722–733 (2014).
2. J. P. Coppé, P. Y. Desprez, A. Krtolica, J. Campisi, The senescence-associated secretory phenotype: The dark side of tumor suppression. *Annu. Rev. Pathol.* **5**, 99–118 (2010).
3. A. Hernandez-Segura, J. Nehme, M. Demaria, Hallmarks of cellular senescence. *Trends Cell Biol.* **28**, 436–453 (2018).
4. J. Jonsson, L. Carlsson, T. Edlund, H. Edlund, Insulin-promoter-factor 1 is required for pancreas development in mice. *Nature* **371**, 606–609 (1994).
5. M. F. Offield, T. L. Jetton, P. A. Labosky, M. Ray, R. W. Stein, M. A. Magnuson, B. L. Hogan, C. V. Wright, PDX-1 is required for pancreatic outgrowth and differentiation of the rostral duodenum. *Development* **122**, 983–995 (1996).
6. M. Horiguchi, M. Yoshida, K. Hirata, K. Furuyama, T. Masui, S. Uemoto, Y. Kawaguchi, Senescence caused by inactivation of the homeodomain transcription factor Pdx1 in adult pancreatic acinar cells in mice. *FEBS Lett. 593*, 2226–2234 (2019).
7. D. G. A. Burton, A. Stolzing, Cellular senescence: Immunosurveillance and future immunotherapy. *Ageing Res. Rev.* **43**, 17–25 (2018).
8. T. W. Kang, T. Yevsa, N. Woller, L. Hoenicke, T. Wuestefeld, D. Dauch, A. Hohmeyer, M. Gereke, R. Rudalska, A. Potapova, M. Iken, M. Vucur, S. Weiss, M. Heikenwalder, S. Khan, J. Gil, D. Bruder, M. Manns, P. Schirmacher, F. Tacke, M. Ott, T. Luedde, T. Longerich, S. Kubicka, L. Zender, Senescence surveillance of pre-malignant hepatocytes limits liver cancer development. *Nature* **479**, 547–551 (2011).
9. D. J. Baker, T. Wijshake, T. Tchkonia, N. K. LeBrasseur, B. G. Childs, B. van de Sluis, J. L. Kirkland, J. M. van Deursen, Clearance of p16Ink4a-positive senescent cells delays ageing-associated disorders. *Nature* **479**, 232–236 (2011).
10. D. J. Baker, B. G. Childs, M. Durik, M. E. Wijers, C. J. Sieben, J. Zhong, R. A. Saltness, K. B. Jeganathan, G. C. Verzosa, A. Pezeshki, K. Khazaie, J. D. Miller, J. M. van Deursen, Naturally occurring $p16^{Ink4a}$-positive cells shorten healthy lifespan. *Nature* **530**, 184–189 (2016).
11. Y. Johmura, T. Yamanaka, S. Omori, T. W. Wang, Y. Sugiura, M. Matsumoto, N. Suzuki, S. Kumamoto, K. Yamaguchi, S. Hatakeyama, T. Takami, R. Yamaguchi, E. Shimizu, K. Ikeda, N. Okahashi, R. Mikawa, M. Suematsu, M. Arita, M. Sugimoto, K. I. Nakayama, Y. Furukawa, S. Imoto, M. Nakanishi, Senolysis by glutaminolysis inhibition ameliorates various age-associated disorders. *Science* **371**, 265–270 (2021).
12. T. W. Wang, Y. Johmura, N. Suzuki, S. Omori, T. Migita, K. Yamaguchi, S. Hatakeyama, S. Yamazaki, E. Shimizu, S. Imoto, Y. Furukawa, A. Yoshimura, M. Nakanishi, Blocking PD-L1-PD-1 improves senescence surveillance and ageing phenotypes. *Nature* **611**, 358–364 (2022).
13. J. A. Ewald, J. A. Desotelle, G. Wilding, D. F. Jarrard, Therapy-induced senescence in cancer. *J. Natl. Cancer Inst.* **102**, 1536–1546 (2010).
14. P. A. Perez-Mancera, A. R. Young, M. Narita, Inside and out: The activities of senescence in cancer. *Nat. Rev. Cancer* **14**, 547–558 (2014).
15. M. Demaria, M. N. O'Leary, J. Chang, L. Shao, S. Liu, F. Alimirah, K. Koenig, C. Le, N. Mitin, A. M. Deal, S. Alston, E. C. Academia, S. Kilmarx, A. Valdovinos, B. Wang, A. de Bruin, B. K. Kennedy, S. Melov, D. Zhou, N. E. Sharpless, H. Muss, J. Campisi, Cellular senescence

promotes adverse effects of chemotherapy and cancer relapse. *Cancer Discov.* **7**, 165–176 (2017).
16. R. Forster, A. E. Mattis, E. Kremmer, E. Wolf, G. Brem, M. Lipp, A putative chemokine receptor, BLR1, directs B cell migration to defined lymphoid organs and specific anatomic compartments of the spleen. *Cell* **87**, 1037–1047 (1996).
17. K. M. Ansel, V. N. Ngo, P. L. Hyman, S. A. Luther, R. Forster, J. D. Sedgwick, J. L. Browning, M. Lipp, J. G. Cyster, A chemokine-driven positive feedback loop organizes lymphoid follicles. *Nature* **406**, 309–314 (2000).
18. W. Zhang, N. Nandakumar, Y. Shi, M. Manzano, A. Smith, G. Graham, S. Gupta, E. E. Vietsch, S. Z. Laughlin, M. Wadhwa, M. Chetram, M. Joshi, F. Wang, B. Kallakury, J. Toretsky, A. Wellstein, C. Yi, Downstream of mutant KRAS, the transcription regulator YAP is essential for neoplastic progression to pancreatic ductal adenocarcinoma. *Sci. Signal.* **7**, ra42 (2014).
19. R. Gruber, R. Panayiotou, E. Nye, B. Spencer-Dene, G. Stamp, A. Behrens, YAP1 and TAZ control pancreatic cancer initiation in mice by direct up-regulation of JAK-STAT3 signaling. *Gastroenterology* **151**, 526–539 (2016).
20. G. Biczo, P. Hegyi, S. Dosa, N. Shalbuyeva, S. Berczi, R. Sinervirta, Z. Hracsko, A. Siska, Z. Kukor, K. Jarmay, V. Venglovecz, I. S. Varga, B. Ivanyi, L. Alhonen, T. Wittmann, A. Gukovskaya, T. Takacs, Z. Rakonczay Jr., The crucial role of early mitochondrial injury in L-lysine-induced acute pancreatitis. *Antioxid. Redox Signal.* **15**, 2669–2681 (2011).
21. B. Zhao, X. Ye, J. Yu, L. Li, W. Li, S. Li, J. Yu, J. D. Lin, C. Y. Wang, A. M. Chinnaiyan, Z. C. Lai, K. L. Guan, TEAD mediates YAP-dependent gene induction and growth control. *Genes Dev.* **22**, 1962–1971 (2008).
22. J. Dong, G. Feldmann, J. Huang, S. Wu, N. Zhang, S. A. Comerford, M. F. Gayyed, R. A. Anders, A. Maitra, D. Pan, Elucidation of a universal size-control mechanism in *Drosophila* and mammals. *Cell* **130**, 1120–1133 (2007).
23. S. Jiao, H. Wang, Z. Shi, A. Dong, W. Zhang, X. Song, F. He, Y. Wang, Z. Zhang, W. Wang, X. Wang, T. Guo, P. Li, Y. Zhao, H. Ji, L. Zhang, Z. Zhou, A peptide mimicking VGLL4 function acts as a YAP antagonist therapy against gastric cancer. *Cancer Cell* **25**, 166–180 (2014).
24. R. Garg, J. M. Blando, C. J. Perez, M. C. Abba, F. Benavides, M. G. Kazanietz, Protein kinase C epsilon cooperates with PTEN loss for prostate tumorigenesis through the CXCL13-CXCR5 pathway. *Cell Rep.* **19**, 375–388 (2017).
25. L. V. Britanova, D. V. Kuprash, New putative control elements in the promoter of the gene for the CXCL13 chemokine, a target of the alternative NF-κB pathway. *Mol. Biol.* **43**, 604–611 (2009).
26. M. L. Chao, S. Luo, C. Zhang, X. Zhou, M. Zhou, J. Wang, C. Kong, J. Chen, Z. Lin, X. Tang, S. Sun, X. Tang, H. Chen, H. Wang, D. Wang, J. P. Sun, Y. Han, L. Xie, Y. Ji, S-nitrosylation-mediated coupling of G-protein alpha-2 with CXCR5 induces Hippo/YAP-dependent diabetes-accelerated atherosclerosis. *Nat. Commun.* **12**, 4452 (2021).
27. G. J. Freeman, A. J. Long, Y. Iwai, K. Bourque, T. Chernova, H. Nishimura, L. J. Fitz, N. Malenkovich, T. Okazaki, M. C. Byrne, H. F. Horton, L. Fouser, L. Carter, V. Ling, M. R. Bowman, B. M. Carreno, M. Collins, C. R. Wood, T. Honjo, Engagement of the PD-1 immunoinhibitory receptor by a novel B7 family member leads to negative regulation of lymphocyte activation. *J. Exp. Med.* **192**, 1027–1034 (2000).
28. T. Okazaki, T. Honjo, PD-1 and PD-1 ligands: From discovery to clinical application. *Int. Immunol.* **19**, 813–824 (2007).
29. C. Lopez-Otin, M. A. Blasco, L. Partridge, M. Serrano, G. Kroemer, The hallmarks of aging. *Cell* **153**, 1194–1217 (2013).
30. L. Zhang, L. E. Pitcher, M. J. Yousefzadeh, L. J. Niedernhofer, P. D. Robbins, Y. Zhu, Cellular senescence: A key therapeutic target in aging and diseases. *J. Clin. Invest.* **132**, e158404 (2022).
31. B. G. Childs, M. Durik, D. J. Baker, J. M. van Deursen, Cellular senescence in aging and age-related disease: From mechanisms to therapy. *Nat. Med.* **21**, 1424–1435 (2015).
32. F. Caldart, N. de Pretis, C. Luchini, R. Ciccocioppo, L. Frulloni, Pancreatic steatosis and metabolic pancreatic disease: A new entity? *Intern. Emerg. Med.* **18**, 2199–2208 (2023).
33. Y. Saisho, A. E. Butler, J. J. Meier, T. Monchamp, M. Allen-Auerbach, R. A. Rizza, P. C. Butler, Pancreas volumes in humans from birth to age one hundred taking into account sex, obesity, and presence of type-2 diabetes. *Clin. Anat.* **20**, 933–942 (2007).
34. M. X. Yan, Y. Q. Li, M. Meng, H. B. Ren, Y. Kou, Long-term high-fat diet induces pancreatic injuries via pancreatic microcirculatory disturbances and oxidative stress in rats with hyperlipidemia. *Biochem. Biophys. Res. Commun.* **347**, 192–199 (2006).
35. E. P. Rogakou, D. R. Pilch, A. H. Orr, V. S. Ivanova, W. M. Bonner, DNA double-stranded breaks induce histone H2AX phosphorylation on serine 139. *J. Biol. Chem.* **273**, 5858–5868 (1998).
36. L. J. Kuo, L. X. Yang, γ-H2AX—A novel biomarker for DNA double-strand breaks. *In Vivo* **22**, 305–309 (2008).
37. C. Feig, A. Gopinathan, A. Neesse, D. S. Chan, N. Cook, D. A. Tuveson, The pancreas cancer microenvironment. *Clin. Cancer Res.* **18**, 4266–4276 (2012).
38. A. E. Vilgelm, A. Richmond, Chemokines modulate immune surveillance in tumorigenesis, metastasis, and response to immunotherapy. *Front. Immunol.* **10**, 333 (2019).
39. J. Xiong, L. Dong, Q. Lv, Y. Yin, J. Zhao, Y. Ke, S. Wang, W. Zhang, M. Wu, Targeting senescence-associated secretory phenotypes to remodel the tumour microenvironment and modulate tumour outcomes. *Clin. Transl. Med.* **14**, e1772 (2024).
40. R. Qu, Y. Zhao, Y. Zhang, The mechanism of cytokine regulation of cancer occurrence and development in the tumor microenvironment and its application in cancer treatment: A narrative review. *Transl. Cancer Res.* **13**, 5649–5663 (2024).
41. Q. Guo, Y. Jin, X. Chen, X. Ye, X. Shen, M. Lin, C. Zeng, T. Zhou, J. Zhang, NF-κB in biology and targeted therapy: New insights and translational implications. *Signal Transduct. Target. Ther.* **9**, 53 (2024).
42. V. A. Garcia-Garcia, J. P. Alameda, A. Page, M. L. Casanova, Role of NF-κB in ageing and age-related diseases: Lessons from genetically modified mouse models. *Cells* **10**, 1906 (2021).
43. F. Du, X. Qi, A. Zhang, F. Sui, X. Wang, C. G. Proud, C. Lin, X. Fan, J. Li, MRTF-A-NF-κB/p65 axis-mediated PDL1 transcription and expression contributes to immune evasion of non-small-cell lung cancer via TGF-β. *Exp. Mol. Med.* **53**, 1366–1378 (2021).
44. A. Di Gregorio, S. Bowling, T. A. Rodriguez, Cell competition and its role in the regulation of cell fitness from development to cancer. *Dev. Cell* **38**, 621–634 (2016).
45. B. Z. Stanger, B. Stiles, G. Y. Lauwers, N. Bardeesy, M. Mendoza, Y. Wang, A. Greenwood, K. H. Cheng, M. McLaughlin, D. Brown, R. A. Depinho, H. Wu, D. A. Melton, Y. Dor, Pten constrains centroacinar cell expansion and malignant transformation in the pancreas. *Cancer Cell* **8**, 185–195 (2005).
46. S. R. Hingorani, E. F. Petricoin, A. Maitra, V. Rajapakse, C. King, M. A. Jacobetz, S. Ross, T. P. Conrads, T. D. Veenstra, B. A. Hitt, Y. Kawaguchi, D. Johann, L. A. Liotta, H. C. Crawford, M. E. Putt, T. Jacks, C. V. Wright, R. H. Hruban, A. M. Lowy, D. A. Tuveson, Preinvasive and invasive ductal pancreatic cancer and its early detection in the mouse. *Cancer Cell* **4**, 437–450 (2003).
47. S. R. Hingorani, L. Wang, A. S. Multani, C. Combs, T. B. Deramaudt, R. H. Hruban, A. K. Rustgi, S. Chang, D. A. Tuveson, Trp53R172H and KrasG12D cooperate to promote chromosomal instability and widely metastatic pancreatic ductal adenocarcinoma in mice. *Cancer Cell* **7**, 469–483 (2005).
48. U. Ahlgren, J. Jonsson, L. Jonsson, K. Simu, H. Edlund, beta-cell-specific inactivation of the mouse Ipf1/Pdx1 gene results in loss of the beta-cell phenotype and maturity onset diabetes. Genes. *Dev*. **12**, 1763–1768 (1998).
49. P. Soriano, Generalized lacZ expression with the ROSA26 Cre reporter strain. *Nat. Genet*. **21**, 70–71 (1999).
50. M. Okabe, M. Ikawa, K. Kominami, T. Nakanishi, Y. Nishimune, 'Green mice' as a source of ubiquitous green cells. *FEBS Lett*. **407**, 313–319 (1997).
51. H. Shibata, S. Komura, Y. Yamada, N. Sankoda, A. Tanaka, T. Ukai, M. Kabata, S. Sakurai, B. Kuze, K. Woltjen, H. Haga, Y. Ito, Y. Kawaguchi, T. Yamamoto, Y. Yamada, In vivo reprogramming drives Kras-induced cancer development. *Nat. Commun*. **9**, 2081 (2018).
52. K. Furuyama, Y. Kawaguchi, H. Akiyama, M. Horiguchi, S. Kodama, T. Kuhara, S. Hosokawa, A. Elbahrawy, T. Soeda, M. Koizumi, T. Masui, M. Kawaguchi, K. Takaori, R. Doi, E. Nishi, R. Kakinoki, J. M. Deng, R. R. Behringer, T. Nakamura, S. Uemoto, Continuous cell supply from a Sox9-expressing progenitor zone in adult liver, exocrine pancreas and intestine. *Nat. Genet*. **43**, 34–41 (2011).
53. M. Sakikubo, K. Furuyama, M. Horiguchi, S. Hosokawa, Y. Aoyama, K. Tsuboi, T. Goto, K. Hirata, T. Masui, Y. Dor, T. Fujiyama, M. Hoshino, S. Uemoto, Y. Kawaguchi, Ptf1a inactivation in adult pancreatic acinar cells causes apoptosis through activation of the endoplasmic reticulum stress pathway. *Sci. Rep*. **8**, 15812 (2018).
54. K. Hirata, S. Kodama, Y. Nakano, Y. Minaki-Nakagawa, Y. Aoyama, M. Sakikubo, T. Goto, M. Yoshida, T. Masui, T. Yamamoto, S. Uemoto, Y. Kawaguchi, Exocrine tissue-driven TFF2 prevents apoptotic cell death of endocrine lineage during pancreas organogenesis. *Sci. Rep*. **9**, 1636 (2019).

Acknowledgments: We thank C. V. E. Wright, Y. Dor, and P. Soriano for providing the *Pdx1* floxed, Elastase-CreER, and Rosa26r mice, respectively. We acknowledge K. Fujii for technical help, K. Okamoto-Furuta and H. Kohda (Division of Electron Microscopic Study, Center for Anatomical Studies, Graduate School of Medicine, Kyoto University) for technical assistance in electron microscopic analysis, and the Division of Histological Study (Center for Anatomical Studies, Graduate School of Medicine, Kyoto University) for technical assistance in histopathological analysis. We thank A. Kakizuka and K. K. Hui for advice on preparing the manuscript. **Funding:** This work was supported by The Grants-in-Aid for Challenging Research (Pioneering), Japan Society for the Promotion of Science (grant no. 18H05384) (Y.K.), Grant-in Aid for Scientific Research (B), Japan Society for the Promotion of Science (grant no. 25K02715) (Y.K.), and The Grants-in-Aid for Challenging Research (Exploratory), Japan Society for the Promotion of Science (grant no. 24K22142) (K.F.). **Author contributions:** Conceptualization: M.Y., C.A., S.N., D.T., and Y.K. Methodology: M.Y., K.S., T.M., Y.Y., S.N., and Y.K. Validation: M.Y., A.I.A.-A., A.M.R., and Y.K. Formal analysis: M.Y., K.S., and Y.K. Investigation: M.Y., K.S., M.H., A.I.A.-A., H.S., A.M.R., T.Y., S.K., and Y.K. Resources: A.T., H.S., S.N., D.T., and Y.K. Data curation: M.Y. and Y.K. Writing—original draft: M.Y. and Y.K. Writing—review and editing: M.Y., K.F., K.S., C.A., S.N., and Y.K. Visualization: M.Y., K.S., and Y.K. Supervision: S.U., E.H., and Y.K. Project administration: Y.K. Funding acquisition: K.F. and Y.K. **Competing interests:** M.Y. is an inventor on a patent application related to this work filed by the author (no. 2026- 42645, filed 17 March 2026). The authors declare that they have no other competing interests.. **Data, code, and**

materials availability: All data and code needed to evaluate and reproduce the results in the paper are present in the paper and/or the Supplementary Materials. Microarray data generated during this study have been deposited in the Gene Expression Omnibus (GEO) with the accession code GSE138498. This study did not generate new materials.

Submitted 21 November 2024
Accepted 27 March 2026
Published 1 May 2026
10.1126/sciadv.adu7865

ScienceAdvances

Stress-induced CXCL13 regulates pancreatic exocrine homeostasis, age-related chronic inflammation, and cancer progression

Masahiro Yoshida, Kenichiro Furuyama, Keisuke Sumide, Masashi Horiguchi, Ahmed I. Abo-Ahmed, Hirofumi Shibata, Akito Tanaka, Ahmed M. Rashwan, Toshihiko Masui, Cantas Alev, Takuya Yamamoto, Yasuhiro Yamada, Shin Kaneko, Shuh Narumiya, David Tuveson, Shinji Uemoto, Etsuro Hatano, and Yoshiya Kawaguchi

Sci. Adv. **12** (18), eadu7865. DOI: 10.1126/sciadv.adu7865

Science Advances (ISSN 2375-2548) is published by the American Association for the Advancement of Science. 1200 New York Avenue NW, Washington, DC 20005. The title *Science Advances* is a registered trademark of AAAS.